



LAWRENCE  
LIVERMORE  
NATIONAL  
LABORATORY

# Deuterium-Hydrogen Exchange in Olivine: Implications for Point Defects and Electrical Conductivity

W. L. Du Frane, J. A. Tyburczy

September 26, 2011

Geochemistry Geophysics Geosystems

## **Disclaimer**

---

This document was prepared as an account of work sponsored by an agency of the United States government. Neither the United States government nor Lawrence Livermore National Security, LLC, nor any of their employees makes any warranty, expressed or implied, or assumes any legal liability or responsibility for the accuracy, completeness, or usefulness of any information, apparatus, product, or process disclosed, or represents that its use would not infringe privately owned rights. Reference herein to any specific commercial product, process, or service by trade name, trademark, manufacturer, or otherwise does not necessarily constitute or imply its endorsement, recommendation, or favoring by the United States government or Lawrence Livermore National Security, LLC. The views and opinions of authors expressed herein do not necessarily state or reflect those of the United States government or Lawrence Livermore National Security, LLC, and shall not be used for advertising or product endorsement purposes.

# **Deuterium-Hydrogen Exchange in Olivine: Implications for Point Defects and Electrical Conductivity**

Wyatt L. Du Frane<sup>1,2</sup> and James A. Tyburczy<sup>1</sup>

<sup>1</sup>School of Earth and Space Exploration, Arizona State University, Tempe, Arizona, USA

<sup>2</sup>Lawrence Livermore National Laboratory, Livermore, California, USA

Knowledge about hydrogen self diffusion ( $D_H$ ) is critical for determining mantle hydrogen distribution and understanding point defects. Also chemical diffusion of hydrogen in olivine, such as redox exchange with polarons ( $D_{\text{Redox}}$ ), depends on  $D_H$ . In this study deuterium  $^2\text{H}$  was exchanged into hydrogen  $^1\text{H}$  saturated single crystals of San Carlos olivine between 750-900 °C at 2 GPa. We measured and fit the resulting  $^2\text{H}$  profiles to obtain  $D_{H,[100]} = 10^{(-4.9 \pm 1.4) * e^{(-140 \pm 30 \text{ kJ/mol})/(RT)}}$   $\text{m}^2/\text{s}$ , which is  $\sim 1$  log unit lower than  $D_{\text{Redox}, [100]}$ , with similar activation enthalpy  $H_a$ . By comparing these two diffusion coefficients, we estimate the small polaron diffusion coefficient. Additionally, we estimate  $D_H$  in the [010] and [001] orientations, demonstrating that  $D_H$  is highly anisotropic in olivine. These  $D_H$  values were used with the Nernst-Einstein relation to estimate the electrical conductivity by hydrogen in olivine ( $\sigma_H = 10^{1.1} * e^{(-130 \text{ kJ/mol})/(RT)}$  S/m for 10<sup>-2</sup> wt% H<sub>2</sub>O) that is lower in magnitude than previous measurements. Our results suggest that hydrogen alone cannot account for high electrical conductivity anomalies observed at asthenospheric depths ( $\sim 10^{-2}$  to  $\sim 10^{-1}$  S/m). The maximum anisotropic variation of  $D_H$  and  $\sigma_H$  in olivine is  $\sim 2$  log units between 750-900 °C, and increases when extrapolated to higher temperature ( $\sim 3.3$  at 1400 °C). Anisotropy observed in the mantle may indicate substantial amounts of hydrogen in olivine with lattice-preferred orientation.

## 1. Introduction

Determining the H<sub>2</sub>O distribution in Earth is essential for understanding mantle flow and for improving interpretations of geophysical data due to the strong influence of hydrogen on the physical and chemical properties of mantle minerals. Hydrogen can occur in significant concentrations as defects in nominally anhydrous minerals. Its presence weakens Si-O bonds,

and as a result affects elastic properties, rheology, phase equilibrium, transport properties, and melting behavior [Jacobsen and van der Lee, 2006; Keppler and Smyth, 2006]. However, the amount of hydrogen present in the mantle is largely unknown.

Estimates of mantle H<sub>2</sub>O content range from essentially dry to 5.5 ocean masses (1 ocean mass =  $1.4 \times 10^{21}$  kg H<sub>2</sub>O) or ~1900 ppmw H<sub>2</sub>O [Hirschmann *et al.*, 2005]. All mantle minerals studied thus far are able to host significant amounts of hydrogen in their crystal structure [Bolfan-Casanova, 2005]. Experimental H<sub>2</sub>O solubility measurements of mantle minerals have underlined important H<sub>2</sub>O storage capacities of mantle mineral assemblages, such as 31,000 ppmw for (Fe,Mg)<sub>2</sub>SiO<sub>4</sub> wadsleyite [Inoue *et al.*, 1995] and 24,000 ppmw for (Fe,Mg)<sub>2</sub>SiO<sub>4</sub> ringwoodite [Kohlstedt *et al.*, 1996].

Hydrogen diffusion in mantle minerals is important for understanding hydrogen transport, mixing, and reservoirs in the mantle. To maintain charge balance in olivine, the presence of hydrogen affects the concentrations, and thus the diffusivities, of other ionic defects (e.g., small polarons, metal- and silicon-vacancies). Chemical diffusion is driven by the presence of a chemical gradient. Kohlstedt and Mackwell [1998] measured hydrogen chemical diffusion coefficients in olivine. They identified two mechanisms to incorporate hydrogen into dry olivine while maintaining stoichiometry: a faster „redox exchange“ mechanism (originally referred to as  $D_{\text{Exch}}$ , but herein referred to as  $D_{\text{Redox}}$  to avoid confusion with deuterium-hydrogen exchange) and a slower „incorporation“ mechanism ( $D_{\text{incorp}}$ ). Redox exchange involves exchange of hydrogen with charged polarons, electron holes (h) created by a ferric iron ion on an octahedral site  $\text{Fe}_{\text{Me}}^\bullet$ .  $D_{\text{Redox}}$  can be expressed as

$$D_{\text{Redox}} = (X_h + X_H) D_h D_H / (X_h D_h + X_H D_H) \quad (1)$$

where  $D_H$  ( $\text{m}^2/\text{s}$ ) is the self diffusivity,  $X_H$  ( $1/\text{m}^3$ ) is the concentration of hydrogen,  $D_h$  ( $\text{m}^2/\text{s}$ ) is the diffusivity, and  $X_h$  ( $1/\text{m}^3$ ) is the concentration of small polarons [Kohlstedt and Mackwell, 1998; 1999]. For special case  $X_h = X_H$  and if  $D_h \gg D_H$  then it follows that  $D_{\text{Redox}} \approx 2 * D_H$ . The slower hydrogen incorporation mechanism involves a simultaneous flow of metal vacancies ( $V_{\text{Me}}$ ) to balance charge [Kohlstedt and Mackwell, 1998; 1999], with chemical diffusivity expressed as

$$D_{\text{Incorp}} = 3 D_{V(\text{Me})} D_H / (2 D_{V(\text{Me})} + D_H) \quad (2)$$

where  $D_{V(\text{Me})}$  ( $\text{m}^2/\text{s}$ ) represents the diffusivity of metal vacancies. If  $D_H \gg D_{V(\text{Me})}$ , then it follows that  $D_{\text{Incorp}} \approx 3 D_{V(\text{Me})}$ . Hydrogen chemical diffusion results can be combined with  $D_H$  values to calculate the diffusivities of  $\text{Fe}_{\text{Me}}^\bullet$  and  $V_{\text{Me}}$  in olivine using equations 1 and 2.  $D_H$  in olivine has only previously been studied indirectly.

In this study we examine deuterium ( $^2\text{H}$ ) - hydrogen ( $^1\text{H}$ ) exchange as an approximation to  $D_H$ . This process involves saturation of samples with  $^1\text{H}$  at pressure and temperature, and then subsequent exchange of the  $^1\text{H}$  with  $^2\text{H}$  at the same conditions. We used secondary ion mass spectroscopy (SIMS) to measure  $^2\text{H}$  and  $^1\text{H}$  concentrations in our samples. Similar to equation 1 for hydrogen-polaron exchange, the diffusion coefficient for  $^2\text{H}$ - $^1\text{H}$  exchange depends on the concentrations of  $^2\text{H}$  ( $X_{^2\text{H}}$ ) and  $^1\text{H}$  ( $X_{^1\text{H}}$ ):

$$D_{^2\text{H}-^1\text{H}} = (X_{^2\text{H}} + X_{^1\text{H}}) D_{^1\text{H}} D_{^2\text{H}} / (X_{^1\text{H}} D_{^1\text{H}} + X_{^2\text{H}} D_{^2\text{H}}) \quad (3)$$

Therefore  $D_{2H-1H}$  varies in value between  $D_{2H}$  and  $D_{1H}$  depending on both time and distance from the edge of the olivine crystal. However absolute rate theory predicts only a small difference between diffusion of  $^2H$  and  $^1H$ , with  $D_{1H} = D_{2H}/\sqrt{2}$ . Therefore we can approximate that  $D_{2H-1H} \approx D_{1H} \approx D_{2H}$ , with only slight underestimation of hydrogen self diffusion coefficient ( $< 0.15$  log units).

In olivine,  $D_H$  (i.e., hydrogen mobility) is high, and therefore has significant contribution  $\sigma_H$  to the overall electrical conductivity of olivine  $\sigma_{Tot}$  [Karato, 1990]. The electrical conductivity of nominally anhydrous olivine  $\sigma_{Dry}$  is dominated by  $Fe_{Me}^\bullet$  and  $V_{Me}$  [Schock *et al.*, 1989; Constable and Roberts, 1997; Du Frane, 2005]. High  $\sigma$  anomalies in some regions of the upper mantle [Filloux, 1980; Oldenburg, 1981; Evans *et al.*, 2005] cannot be explained by dry olivine and have instead been attributed to grain boundary phases, melting [e.g., Shankland and Waff, 1977; Shankland *et al.*, 1981], and/or hydrogen [Karato, 1990]. Published measurements agree that hydrogen significantly enhances the  $\sigma$  of upper mantle and transition zone minerals, but differ on how much and by what mechanism(s) hydrogen contributes [Huang *et al.*, 2005; Wang *et al.*, 2006; Yoshino *et al.*, 2006; 2009; Manthilake *et al.*, 2009; Romano *et al.*, 2009; Poe *et al.*, 2010].

$D_H$  can provide a different perspective on how  $\sigma_H$  affects  $\sigma_{Tot}$  with information exclusively on hydrogen mobility.  $D_H$  and  $\sigma_H$  are related by the Nernst-Einstein relation

$$\sigma_{H,[hkl]} = f D_{H,[hkl]} C_H q^2 / (kT) \quad (4)$$

where  $f$  is a unitless numerical correlation factor approximately equal to 1,  $D_{H,[hkl]}$  is the hydrogen self diffusion coefficient ( $m^2/s$ ) in crystallographic direction  $hkl$ ,  $C_H$  is concentration of

hydrogen ( $1/\text{m}^3$ ),  $q$  (C) is charge,  $k$  (J/K) is the Boltzmann constant, and  $T$  (K) is temperature. *Karato* [1990] predicted  $\sigma_{\text{H}}$  in olivine using chemical diffusion coefficients with equation 4. We improve this effort by applying our more appropriate measurements of  $D_{\text{H}}$ . This approach assumes  $\sigma_{\text{H}}$  occurs by self diffusion of all hydrogen as ions (i.e protons), but does not account for the possibility of hydrogen speciation, where different species could have different mobilities or charge depending on site (i.e.,  $\text{H}_i^\bullet$ ,  $\text{H}_{\text{Me}}$ , and  $(2\text{H})_{\text{Me}}^{\times}$ ) [*Karato*, 2006]. However, the Nernst-Einstein relation provides a valuable end member case for comparing  $D_{\text{H}}$  to  $\sigma$  measurements on hydrous minerals. Our model indicates that  $\sigma_{\text{H}}$  is highly anisotropic and has significant contribution to electrical conductivity of olivine, but is unable to account for high magnitude  $\sigma$  anomalies that have are observed in the asthenosphere.

## **2. Experimental Techniques**

### **2.1. Sample preparation**

Crack- and inclusion-free pieces of a single crystal of San Carlos olivine were selected from the same large crystal used for previous studies on  $\sigma_{\text{Dry}}$  [*Du Frane*, 2005; *Du Frane et al.*, 2005]. Electron microprobe analysis indicates a composition of  $\text{Fo}_{89.1}$ . The crystal was oriented through optical microscopy and Laue back-reflection X-ray diffraction. It was then cut within  $\pm 5^\circ$  of each principal axis to make several orthorhombic parallelepiped shaped samples with  $\sim 2.0$  mm length parallel to the  $[100]$  direction,  $\sim 1.5$  mm length parallel to  $[001]$ , and  $\sim 1.0$  mm length parallel to  $[010]$  in the  $\text{Pbnm}$  space group. These lengths allowed us to track orientation and obtain 1-D diffusion information for all 3 orientations in each experimental run.

### **2.2. Experimental Design**

Experiments consisted of three steps: 1) a „dry anneal“ to set a homogenous population of anhydrous point defects, 2) a „wet anneal“ to saturate samples with hydrogen, 3) an „exchange anneal“ to exchange  $^2\text{H}$  for  $^1\text{H}$ .

Control of point defect chemistry was achieved with a „dry anneal“ in a 1-atm gas mixing furnace at 1300 °C for > 15 hours (Table 1). We used a  $\text{CO}_2\text{:CO}$  gas mixture to control  $f_{\text{O}_2}$  at that of the Ni-NiO buffer (NNO). This step fixed the concentrations of defects in the metal sublattice (*e.g.*, oxygen-, silicon-, and metal- vacancies or interstitial defects), where high temperature was required because of relatively slow diffusion in comparison to hydrogen or polarons [*e.g.*, *Kohlstedt and Mackwell*, 1998].

A „wet anneal“ was then performed in a piston cylinder device with  $^1\text{H}_2\text{O}$  to saturate the olivine with  $^1\text{H}$  at 2.00  $\pm$  0.05 GPa and 750-900 ( $\pm$  2) °C for 16-48 hours. Durations varied with temperature (Table 1), and were sufficient to saturate hydrogen throughout the crystal via the redox exchange mechanism [*Kohlstedt and Mackwell*, 1998]. Samples plus  $\text{H}_2\text{O}$  were contained in a 1 mm thick-walled silver capsule lined with 0.13 mm thick gold. Olivine powder (sieved to < 20  $\mu\text{m}$ ) was included to prevent dissolution of the sample.  $\text{SiO}_2$  was buffered by inclusion of a few San Carlos enstatite crystals, and  $f_{\text{O}_2}$  was buffered using Ni foil separated from samples by a  $\text{Ag}_{30}\text{Pd}_{70}$  foil membrane [*Diedrich et al.*, 2009]. The fluid also provides a hydrostatic pressure medium to reduce impingement or crushing of samples. Pressure and temperature were increased and subsequently decreased together to follow an approximately isochoric P-T path to reduce sample fracture or capsule leaks.

In the final „exchange anneal“  $^2\text{H}$  and  $^1\text{H}$  were exchanged under identical pressure/temperature/ $f_{\text{O}_2}$  conditions as the previous „wet anneal“ of the individual samples. The bath consisted of  $\sim 9^2\text{H}_2\text{O}:1^1\text{H}_2\text{O}$  by weight and the runs were 10-60 minutes duration. Samples were initially pressurized to 2 GPa and heated to 500 °C simultaneously. From 500 °C the target temperature was reached in less than 5 minutes. Runs were finished by cutting power off to the heaters such that the temperature reduced to < 500 °C in seconds. Recovered samples were cut into two pieces and polished (1  $\mu\text{m}$ ) in two different perpendicular directions to expose two faces, each containing 2 of 3 principal orientations.

### 3. Secondary Ion Mass Spectrometry

Determination of the post-run  $^1\text{H}$  and  $^2\text{H}$  profiles were obtained by performing SIMS on sectioned samples using the Cameca 6f at the ASU National SIMS Facility (<http://sims.asu.edu>). SIMS provides beam diameters of a few microns with usable primary currents and sensitivity of  $\sim 10\text{-}100 \text{ H}/10^6 \text{ Si}$  in silicon [Hauri *et al.*, 2002; Koga *et al.*, 2003; Aubaud *et al.*, 2007]. A primary beam of cesium ions sputtered and accelerated negative secondary ions into the mass spectrometer, creating  $\sim 8 \mu\text{m}$  diameter craters restricted by a field aperture for regional spot analysis (Figure 1).

We used hydrogen in olivine standards previously studied by Tenner *et al.* [2009] for some preliminary experiments, but the majority of data in this study was collected “standardless”. Du Frane [2010] measured  $75 \pm 15 \text{ ppmw H}_2\text{O}$  (or  $\sim 1500 \text{ H}/10^6 \text{ Si}$ ) in olivine surrounded by liquid  $\text{H}_2\text{O}$  at 2 GPa, 950 °C, for 48 hours; but these samples did not undergo a „dry anneal“ step. Hydrogen solubility in olivine varies from  $1000\text{-}2400 \text{ H}/10^6 \text{ Si}$  ( $\sim 50\text{-}120$

ppmw H<sub>2</sub>O) at 2 GPa, between 750 – 900 °C [Zhao *et al.*, 2004; using water fugacity values from Pitzer and Sterner, 1994]. Hydrogen contents of the olivine samples in this study largely depend on the metal sublattice fixed by the high temperature „dry anneal“, and are therefore likely to have less temperature variation than solubility measurements. Absolute concentrations are not required to determine diffusion coefficients. The most critical data are ion intensities for <sup>16</sup>O<sup>1</sup>H and <sup>16</sup>O<sup>2</sup>H in the interior (low <sup>16</sup>O<sup>2</sup>H, high <sup>16</sup>O<sup>1</sup>H) and the edge (high <sup>16</sup>O<sup>2</sup>H, low <sup>16</sup>O<sup>1</sup>H) of the olivine crystal. Further details on SIMS analyses are in Supplement Section S1. Due to lack of calibrations we cannot quantitatively balance <sup>1</sup>H + <sup>2</sup>H; however, samples exhibit qualitative relationships of <sup>1</sup>H diffusing out of and <sup>2</sup>H diffusing into the crystal (See Figure S1 in Supplement Section S1).

#### 4. Results

Wet/exchange anneals were performed at 2 GPa and temperatures of 750 (PC25), 800 (PC28), 850 (PC30), and 900 °C (PC33). Samples generally experienced some fracturing on mechanically weak edges and corners, but we were able to track orientation for samples PC25, PC28, and PC33. Sample PC30 was more fractured, and we lost track of the orientation.

Diffusion profiles were collected for <sup>1</sup>H and <sup>2</sup>H for each principal orientation of each sample. Profiles consisted of an array of spot analyses plotted versus distance from the nearby, oriented edge of interest, while being sufficiently far from other edges (Figure 1). <sup>1</sup>H diffused out and <sup>2</sup>H diffused into olivine and enstatite (Figure S1 in Supplement Section S1). This verifies that <sup>2</sup>H exchanged with <sup>1</sup>H in our experiments, demonstrating that the diffusion coefficients we have measured are good approximations of self diffusion coefficients. SIMS results indicate that

<sup>2</sup>H diffused the furthest in the [100] direction at each temperature (Figure 2). Experiments were short enough in duration to prevent diffusion of <sup>2</sup>H to the center, so that data in the slower [010] and [001] directions were not affected by diffusion in the fastest [100] direction. Short diffusion lengths in the [010] and [001] directions limited the analysis of diffusion profiles for these directions.

<sup>2</sup>H profiles were analyzed using 1-D solutions to Fick's second law for a semi-infinite solid [Carslaw, 1959; Crank, 1975; Ingrin and Skogby, 2000]. Concentration along the x-direction perpendicular to the surface is

$$\frac{C(x,t)-C_0}{C_1-C_0} = \text{erfc}\left(\frac{x}{2\sqrt{D_H t}}\right) \quad (5)$$

where  $C(x,t)$  (<sup>16</sup>O<sup>2</sup>H/<sup>30</sup>Si) is concentration at distance  $x$  (m) and time  $t$  (s),  $C_0$  is the initial concentration (set to zero), and  $C_1$  is the concentration at the sample boundary. Errors in diffusion coefficient were determined as +/- one standard deviation from the least squared fitting solutions (Figure 2 insets). <sup>1</sup>H was not included in fits to determine  $D_H$  because of the relatively larger error in these data. A full 3-D analysis [Demouchy and Mackwell, 2003] was not necessary because our results indicate that  $D_{H,[100]} \gg D_{H,[001]}, D_{H,[010]}$ . We fit diffusion coefficients (weighted by error) to the Arrhenius equation to determine the preexponential term  $D_{0,[100]}$  (m<sup>2</sup>/s) and activation enthalpy  $H_{a,[100]}$  (kJ/mol)

$$\text{Log}(D_{H,[100]}(T)) = \text{Log}(D_{0,[100]}) - \frac{H_{A,[100]}}{2.303 \cdot RT} \quad (6)$$

where  $R$  is the gas constant. For <sup>2</sup>H-<sup>1</sup>H exchange in olivine at 2 GPa between 750-900 °C, we determined  $D_{0,[100]} = 10^{(-4.9 \pm 1.4)} \text{ m}^2/\text{s}$  and  $H_{A,[100]} = 140 \pm 30 \text{ kJ/mol}$  (Figure 3).

For  $D_H$  in the [010] and [001] orientations we fixed the boundary condition ( $C_1$ ) to those values derived from [100] fits (labeled „anchor“ in Figure 2D). We determined  $D_{H,[001]} = 10^{-12.0 \pm 0.2} \text{ m}^2/\text{sat } 900^\circ\text{C}$  (Figure 3). Spatial resolution was insufficient to resolve diffusion profiles for [010] and for [001] below  $900^\circ\text{C}$ . In these cases maxima for diffusion coefficients were estimated (Table 1, Figure S1 in Supplement Section S1). These maxima validate our treatment of [100] diffusion data as 1-D (equation 5). Diffusion coefficients were also estimated in 3 non-oriented directions in a bisection of the PC30 olivine sample (Table 1).

Useful information about polaron diffusion and electrical conductivity can be inferred from comparison of measurements of  $D_{\text{Redox}}$  and  $D_H$ , however we must consider the pressure differences between these two studies, which were conducted at 0.3 and 2.0 GPa respectively. Activation enthalpy has the following dependence on pressure:

$$H_a = E_a + P\Delta V_a \quad (7)$$

where  $E_a$  is activation energy,  $P$  is pressure, and  $\Delta V_a$  is activation volume. Activation volume ( $\Delta V_a$ ) for  $D_{\text{Redox}}$  and  $D_H$  are poorly constrained; however the  $H_a$  value we calculate for  $D_{H,[100]}$  ( $140 \pm 30 \text{ kJ/mol}$ ) is nearly identical to that of  $D_{\text{Redox},[100]}$  ( $145 \pm 30 \text{ kJ/mol}$ ). This suggests that activation volume is small, and we assume that  $\Delta V_a \approx 0$  in the following calculations.

Although limited data were obtained for  $D_{H,[010]}$  and  $D_{H,[001]}$  from our experiments, we estimate their values and  $D_{h,[100]}$  using equation 1, which be rearranged algebraically to solve for  $D_h$ ,  $D_H$ ,  $X_h$ , and  $X_H$ ; the requirement that these quantities be positive yields several constraints (See Supplement Section S2). We combine these with our result  $D_{\text{Redox},[100]}/D_{H,[100]} \approx 10^{0.86} = 7.24$  to obtain the following constraints:

$$0 < X_h < 0.16 * X_H \quad (8a)$$

$$D_{Redox} < D_h < 625 * D_{Redox} \quad (8b)$$

Although we do not have measured values for  $X_h$  and  $D_h$  as they pertain to the samples used to measure  $D_{Redox}$ , we can use these constraints to make a reasonable estimates. *Kohlstedt and Mackwell* [1999] approximate that  $X_H \leq X_h$  throughout their samples over the entire duration of their experiments, however this conflicts with constraints given in equation 8a. These can only be satisfied if the majority of polarons exchanged with hydrogen near the edges of their samples during the experiments, which implies that boundary values of  $X_h$  and  $X_H$  towards the end of their experiments largely determine the constant  $D_{Redox}$  values they fit. We approximate  $X_h = 0.08 * X_H$ , the middle of the range constrained by equation 8a.

Using this ratio between  $X_h$  and  $X_H$  along with measurements of  $D_{H,[100]}$  and  $D_{Redox,[100]}$  we use equation 1 to calculate  $D_{h,[100]} = 10^{-3.8} * e^{(-140 \text{ kJ/mol})/(RT)} \text{ m}^2/\text{s}$ .  $D_h$  must be greater than  $D_{Redox,[100]}$  as required by equation 1 (See Supplement Section S2 for derivation), and is slightly greater than that calculated for polycrystalline San Quintin Dunite [*Constable and Roberts* 1997] (Figure 3). There is little anisotropy for  $\sigma_{Dry}$  ( $< 0.3$  log units) which is believed to be dominated by small polarons for temperature less than  $\sim 1300$  °C [*Schock et al.*, 1989; *Du Frane*, 2005; *Du Frane et al.*, 2005], therefore we can use the approximation  $D_{h,[100]} \approx D_{h,[010]} \approx D_{h,[001]}$ . Using  $D_{h,[100]}$  along with  $D_{Redox,[010]}$  and  $D_{Redox,[001]}$  in equation 1 we calculate  $D_{H,[010]} = 10^{-5.4} * e^{(-170 \text{ kJ/mol})/(RT)} \text{ m}^2/\text{s}$  and  $D_{H,[001]} = 10^{-8.4} * e^{(-100 \text{ kJ/mol})/(RT)} \text{ m}^2/\text{s}$  (Figure 3). These calculations are in fairly good agreement with our measured and estimated values for  $D_{H,[001]}$  and estimated values for  $D_{H,[010]}$  (Figure 4, Table 1).

From  $D_H$  in olivine we construct a  $\sigma_H$  model as a function of  $H_2O$  content and temperature using equation 4. Measurement of  $D_{H,[100]}$  and calculations of  $D_{H,[010]}$  and  $D_{H,[001]}$  are combined with equation 4 to calculate  $\sigma_{H,[100]}$ ,  $\sigma_{H,[010]}$ , and  $\sigma_{H,[001]}$  respectively, with geometric mean  $\sigma_H = 10^{1.1} * e^{(-130 \text{ kJ/mol})/(RT)}$  S/m for  $10^{-2}$  wt%  $H_2O$  (Figure 4a and 4b; See Supplement Section S3).  $\sigma_H$  in olivine is combined with  $\sigma_{dry}$  (NNO) to calculate  $\sigma_{Tot}$  in each principal orientation (See Supplement Section S3) (Figure 4c and 4d). For nominally anhydrous olivine, we use the  $\sigma$  model from [Du Frane *et al.*, 2005]. This study used samples cut from the same large San Carlos olivine crystal. Extrapolation of  $\sigma_{Dry}$  from single crystal studies [e.g., Du Frane *et al.*, 2005] to lower temperature and reduced  $f_{O_2}$  results in high  $\sigma$  relative to polycrystalline, nominally anhydrous olivine [e.g., Constable *et al.*, 1992, Roberts and Duba, 1995, Xu *et al.*, 1998]. For comparison to the range of reported values for  $\sigma_{dry}$  we also show  $\sigma_{Tot}$  calculation using the SEO3 model [Constable, 2006] (Figures 4c and 4d). We calculate  $\sigma_H$  and  $\sigma_{Tot}$  for polycrystalline olivine that are lower than those inferred from measurements by Wang *et al.* [2006] and more similar in magnitude to those of Yoshino *et al.* [2009] and Poe *et al.* [2010], (Figure 4).

Diffusion coefficients for  $^2H$ - $^1H$  exchange were also measured in non-oriented, single crystal San Carlos enstatite  $D_{H, En}$  at 2 GPa and 750-900 °C (Table 1). „Dry anneals“ were not performed on enstatite samples. For PC33 at 2 GPa and 900 °C,  $D_{H, En}$  values were calculated along 3 orthogonal directions parallel ( $\pm 10^\circ$ ) to the optical extinction angles of one enstatite sample.  $D_{H, En}$  are  $10^{-11.7 \pm 0.3}$  m<sup>2</sup>/s for directions 1 and 2, and  $10^{-12.0 \pm 0.3}$  m<sup>2</sup>/s in direction 3; this indicates a maximum anisotropic variation of  $\sim 0.3$  log units.  $D_{H, En} = 10^{-13.2 \pm 0.1}$  m<sup>2</sup>/s at 2 GPa

and 800 °C, which ranges between that of synthetic and synthetic, Cr-doped (~0.6 wt%) enstatite [Stalder and Behrens, 2006].

## 5. Discussion

*Kohlstedt and Mackwell* [1999] show that for the special case  $X_h = X_H$  and if  $D_h \gg D_H$  then  $D_{\text{Redox}} \approx 2 \cdot D_H$ , and other authors [e.g., *Demouchy and Mackwell*, 2006] have used this last relationship. We measure  $D_{H, [100]}$  for olivine at 2 GPa that is a factor of 7.2 (or 0.86 log units) lower than  $D_{\text{Redox}, [100]}$  (at 0.3 GPa) (Figure 3), therefore our results indicate that these conditions are not met for  $\Delta V_a \approx 0$ . Alternatively, we calculate that  $\Delta V_a = -RT \cdot \{\partial \ln(D_{H, [100]}) / \partial P\}_T \approx 7 \times 10^{-6} \text{ m}^3$  would satisfy the condition that  $D_{\text{Redox}} \approx 2 \cdot D_H$  for both pressures. Our results indicate that  $D_H \gg D_{V(\text{Me})}$  which supports the conclusion by *Kohlstedt and Mackwell* [1998] that  $D_{\text{Incorp}} \approx 3D_{V(\text{Me})}$ .

We use  $D_{H, [100]}$  and  $D_{\text{Redox}, [100]}$  to calculate  $D_{h, [100]}$ . *Sato* [1986] extrapolated data from *Misener* [1973] to  $\text{Fo}_{92}$  composition to derive a value of  $D_h = 3 \times 10^{-9} \text{ m}^2/\text{s}$  at 1400 °C; extrapolation of our calculation to 1400 °C gives excellent agreement with  $D_{h, [100]} = 7 \times 10^{-9} \text{ m}^2/\text{s}$ . The values we calculate for  $D_{H, [100]}$  are also in good agreement with  $D_h = 1 \times 10^{-9} \text{ m}^2/\text{s}$  at 1400 °C modeled from 1-atm  $\sigma$  and thermopower measurements of dry, fine grained, polycrystalline olivine [*Roberts and Duba*, 1995; *Constable and Roberts*, 1997] (Figure 3).

In olivine,  $D_H$  and  $\sigma_H$  are highly anisotropic with a maximum variation of ~2 log units (Figure 3, Table 1). For enstatite the maximum anisotropic variation of  $D_H$  is only ~0.3 log units at 900 °C (Table 1), suggesting that  $\sigma_H$  in enstatite would make only a small contribution to mantle anisotropy. Magnetotelluric results from different tectonic environments indicate

270 electrical anisotropies of  $\sim 0.4$  to  $> 2.0$  log units in the mantle [Bahr and Simpson, 2002;  
271 Leibecker et al., 2002; Simpson, 2002]. It has been suggested that mantle anisotropy results from  
272 lattice preferred orientation of hydrous olivine [e.g., Zhang and Karato, 1995; Simpson and  
273 Tommasi, 2005]. Our results for olivine between 750-900 °C are consistent with the lower range  
274 of anisotropy observed in the mantle. However extrapolation of  $D_H$  to higher temperature results  
275 in larger maximum anisotropic variation of  $\sigma_H$  ( $\sim 3.4$  log units at 1400 °C).  $C_{H_2O}$  would have to  
276 be very large for  $\sigma_H$  to dominate  $\sigma_{Tot}$ , which means that high degrees of mantle conductivity  
277 anisotropy could indicate the presence of large amounts of hydrogen (Figure 5a).

278 Magnetotelluric surveys have observed high  $\sigma$  ranging between  $10^{-2}$ - $10^{-1}$  S/m at  
279 asthenospheric depths [Lizarralde et al., 1995; Olsen, 1999; Ichiki et al., 2001; Tarits et al.,  
280 2004; Baba et al., 2006], and this has been attributed to hydrogen conduction [e.g., Karato,  
281 1990]. Olivine can accommodate up to  $\sim 1000$ - $2000$  ppmw  $H_2O$  ( $\sim 20,000$ - $40,000$  H/ $10^6$ Si) at  
282 asthenospheric conditions ( $\sim 100$ - $200$  km depth,  $\sim 1300$ - $1400$  °C) [Mosenfelder et al., 2006]. We  
283 compare our  $\sigma_{Tot}$  model for olivine with various hydrogen contents to these values (Figure 5b).  
284 Our model implies that the lower range of conductivity values could be explained by  $\sim 10^2$ - $10^3$   
285 ppmw  $H_2O$ . The highest asthenospheric  $\sigma$  would require  $H_2O$  ( $\sim 10^4$  ppmw) exceeding solubility  
286 measurements for olivine. This contrasts with the estimate of Wang et al. [2006] that 80 ppmw  
287  $H_2O$  ( $\sim 1500$  H/ $10^6$ Si) can account for highest magnitude asthenospheric  $\sigma$  anomalies. The  
288 inability of hydrogen to account for these anomalies necessitates an additional or different  
289 contribution to  $\sigma$ , such as melting or grain boundary phases [e.g., Shankland et al., 1981;  
290 Yoshino et al., 2006; Yoshino et al., 2010].

Wang *et al.* [2006] and Huang *et al.* [2005] suggested that a small fraction of highly mobile free protons dominate  $\sigma_H$  yielding

$$\sigma_H = AC_{H_2O}^r e^{\frac{-H_a}{RT}} \quad (9)$$

where A (S/m) is a preexponential term,  $C_{H_2O}$  is concentration of  $H_2O$  (ppmw), and r is a unitless exponent ranging from 0.50-0.75. Huang *et al.* [2005] proposed an ionization reaction for neutral proton pairs on metal vacancies  $(2H)_M^X$  where



where  $H_M$  is hydrogen on a metal vacancy site, which does not contribute to  $\sigma$  because of its low mobility, and  $H^\bullet$  is a less abundant interstitial species of hydrogen with high mobility. This contrasts with equation 4 which treats all hydrogen as contributing equally to  $\sigma$ . Karato [2006] argued that multiple species of hydrogen exist in olivine, such that hydrogen diffusion coefficients are dominated by the migration of the more-abundant, less-mobile species of hydrogen (neutral  $(2H)_{Me}^X$ ), and electrical conductivity is dominated by a less-abundant, more-mobile species of hydrogen (free protons,  $H^\bullet$ ) [Huang *et al.*, 2005; Wang *et al.*, 2006]. If this were true we would expect that a small population of free  $^2H$  (~5-10 ppmw based on equation 9 with reported  $r = 0.50-0.75$  [Wang *et al.*, 2006]) would have diffused homogenously throughout our samples given the high diffusion coefficient of free hydrogen inferred from Wang *et al.* [2006]:  $\sim 10^{-9}-10^{-7}$  m<sup>2</sup>/s at 900 °C. This quantity (~5-10 ppmw) is only slightly above our  $^2H$  detection limit using SIMS (~5 ppmw  $^2H_2O$ ), nevertheless we see no evidence of  $^2H$  in the center of our samples. However if  $^2H^\bullet$  exchanges with  $^1H^\bullet$  and has high mobility, then

exchange between  $^2\text{H}^\bullet$  and  $^1\text{H}_{\text{Me}}$  or  $(2\ ^1\text{H})_{\text{Me}}^x$  seems likley, which would lead to even higher concentrations of  $^2\text{H}$  in the center of our samples. In this case  $^2\text{H}$  exchange might be dominated by the most mobile species rather than the most abundant species of  $^2\text{H}$ ; however, this is inconsistent with the magnitude of our  $D_{\text{H}}$  values.

Alternatively, *Yoshino et al.* [2009] proposed a model for  $\sigma_{\text{H}}$  in olivine that treats all hydrogen as a single charge-carrying species with one value of mobility. They express  $\sigma_{\text{H}}$  as

$$\sigma_{\text{H}} = \sigma_0 C_{\text{H}_2\text{O}} e^{\left( \frac{-H_a + C_{\text{H}_2\text{O}}^{\frac{1}{3}}}{RT} \right)} \quad (11)$$

where  $\sigma_0$  (S/m) is a pre-exponential term, and  $H_a$  is a fitting parameter. All hydrogen contributes equally to  $\sigma$ , similar to equation 4; however, measurements by *Yoshino et al.* [2009] indicate that  $H_a$  depends on  $C_{\text{H}_2\text{O}}$  content, with an additional term  $\alpha C_{\text{H}_2\text{O}}^{\frac{1}{3}}$  to correct for this. *Poe et al.* [2010] report results similar to *Yoshino et al.* [2006, 2009]; equation 11 fit their data better than equation 9. However, their results suggest that  $H_a$  has an even stronger dependence on  $C_{\text{H}_2\text{O}}$ . *Poe et al.* [2010] suggest that the discrepancy may be due to underestimation of  $C_{\text{H}_2\text{O}}$  by a factor of  $\sim 4$  from use of the FTIR calibration by *Paterson* [1982] instead of more recent calibration [*Bell et al.*, 2003; see also *Mosenfelder et al.*, 2006]. We are unable to determine if  $H_a$  has dependence on  $C_{\text{H}_2\text{O}}$ , because our experiments only covered a limited range of  $C_{\text{H}_2\text{O}}$ .

Experimentally determined  $H_a$  from  $\sigma$  measurements should reflect changes to hydrogen mobility with temperature, assuming  $C_{\text{H}_2\text{O}}$  does not change significantly during heating and cooling cycles. Equation 4 assumes that hydrogen mobility is proportional to  $D_{\text{H}}/T$ ; if correct,  $H_a$

should be similar for both  $D_H$  and  $\sigma_H$ . For  $\text{Log}(C_{H_2O}) = -2$  ( $C_{H_2O}$  in wt %  $H_2O$ ),  $H_a$  calculated by Wang *et al.* [2006], Yoshino *et al.* [2009], and Poe *et al.* [2010] are quite similar ( $\sim 90$  kJ/mol) and lower than those of both  $D_{H,[100]}$  ( $140 \pm 30$  kJ/mol) and  $\sigma_H$  (130 kJ/mol) in this study, and  $D_{\text{Redox}}$  in olivine (110-180 kJ/mol) [Kohlstedt and Mackwell, 1998]. This discrepancy could be due in part to experimental pressure differences amongst these studies, where measurements of activation volume are needed to improve comparisons of these studies. Another possible explanation for variations in reported  $H_a$  values may be variations of  $C_{H_2O}$  in samples during temperature cycling in the  $\sigma$  experiments.  $f_{H_2O}$  and hydrogen solubility in olivine decrease with increasing temperature, and vice versa. Hydrous olivine samples in such studies cannot be isolated so hydrogen may exchange reversibly with adjacent assembly materials, which would make hysteresis of  $\sigma_H$  minimal, and cause underestimation of  $H_a$  associated with  $\sigma_{\text{Tot}}$  measurements.

## 6. Conclusions

We measured  $D_H$  in olivine and enstatite from  $^2H$ - $^1H$  exchange experiments at 2 GPa and 750-900 °C. Hydrogen self diffusion is highly anisotropic, with  $D_{H,[100]} \gg D_{H,[001]}, D_{H,[010]}$ . We measured  $D_{H,[100]}$  in olivine that is a factor of 7.2 (or 0.86 log units) lower than  $D_{\text{Redox},[100]}$ , and both had similar  $H_a$ . For the previous estimate that  $D_{\text{Redox}} \approx 2 \cdot D_H$  to hold for our measurements of  $D_{H,[100]}$  at 2 GPa, an activation volume of  $\sim 7 \times 10^{-6} \text{ m}^3$  is required. Measurements of activation volume for hydrogen diffusion and conduction in olivine are needed to improve comparisons of our  $D_H$  results to other studies.

Measurements and estimates of  $D_H$  values were used with the Nernst-Einstein relation (along with results for nominally anhydrous olivine) to model the total  $\sigma$  of hydrous olivine. Our model suggests that hydrogen makes significant contributions to overall  $\sigma$ , but the conductivity values are slightly lower than those of *Yoshino et al.* [2006], *Yoshino et al.* [2009], and *Poe et al.* [2010]; and 2-3 orders of magnitude lower than that of *Wang et al.* [2006]. Our model suggests that hydrogen is unable to account for  $\sigma$  anomalies observed at asthenospheric depths, but could account for the range of anisotropy in  $\sigma$  observed in the upper mantle if hydrogen was abundant.

### Acknowledgements

We thank A. Pommier, S. Karato, S. Mackwell, J. Boyce, D. Hasterock, and S. Heath for useful comments and discussion; T. Tenner, A. Withers, and M. Hirschmann for their assistance with SIMS and calibration; T. Diedrich, G. Moore, and T. Sharp for help with piston cylinder experiments conducted in the ASU OmniPressure lab; and D. Kohlstedt, and an anonymous reviewer for comments that greatly improved the manuscript. This work was supported by NSF EAR 0739050 to J. A. Tyburczy and R. Hervig. SIMS data were obtained at the ASU National SIMS Facility, supported by NSF EAR 0622775 to R. Hervig & P. Williams. Prepared by LLNL under Contract DE-AC52-07NA27344.

### References

Aubaud, C., A. C. Withers, M. M. Hirschmann, Y. Guan, L. A. Leshin, S. J. Mackwell, and D. R. Bell (2007), Intercalibration of FTIR and SIMS for hydrogen measurements in glasses and nominally anhydrous minerals, *Amer. Mineral.*, 92(5-6), 811-828.

370 Baba, K., A. D. Chave, R. L. Evans, G. Hirth, and R. L. Mackie (2006), Mantle dynamics  
 371 beneath the East Pacific Rise at 17 degrees S: Insights from the Mantle Electromagnetic and  
 372 Tomography (MELT) experiment, *J. Geophys. Res. [Solid Earth]*, *111*, B02101, doi:  
 373 10.1029/2004JB003598.

374 Bahr, K., and F. Simpson (2002), Electrical anisotropy below slow- and fast-moving plates:  
 375 Paleoflow in the upper mantle?, *Science*, *295*(5558), 1270-1272.

376 Bell, D. R., G. R. Rossman, J. Maldener, D. Endisch, and F. Rauch (2003), Hydroxide in olivine:  
 377 A quantitative determination of the absolute amount and calibration of the IR spectrum, *J.*  
 378 *Geophys. Res. [Solid Earth]*, *108*, 2105, doi: 10.1029/2001JB000679.

379 Bolfan-Casanova, N. (2005), Water in the Earth's mantle, *Mineral. Mag.*, *69*(3), 229-257.

380 Carslaw, H. S. and J. C. Jaeger (1959), *Conduction of Heat in Solids*, Oxford University Press.

381 Constable, S. (2006), SEO3: A new model of olivine electrical conductivity, *Geophys. J. Int.*,  
 382 166, 435-437.

383 Constable, S., and J. J. Roberts (1997), Simultaneous modeling of thermopower and electrical  
 384 conduction in olivine, *Phys. Chem. Miner.*, *24*(5), 319-325.

385 Constable, S., T. J. Shankland, A. Duba (1992), The electrical conductivity of an olivine mantle,  
 386 *J. Geophys. Res.*, *97*, 3397-3404.

387 Crank, J. (1975), *The Mathematics of Diffusion*, Oxford University Press.

388 Demouchy, S., and S. Mackwell (2003), Water diffusion in synthetic iron-free forsterite, *Phys.*  
 389 *Chem. Miner.*, *30*(8), 486-494.

390 Demouchy, S., and S. Mackwell (2006), Mechanisms of hydrogen incorporation and diffusion in  
 391 iron-bearing olivine, *Phys. Chem. Miner.*, *33*, 347-355.  
 392 Diedrich, T., T. G. Sharp, K. Leinenweber, and J. R. Holloway (2009), The effect of small  
 393 amounts of H<sub>2</sub>O on olivine to ringwoodite transformation growth rates and implications for  
 394 subduction of metastable olivine, *Chem. Geol.*, *262*(1-2), 87-99.  
 395 Du Frane, W. L. (2005), Anisotropic Electrical Properties of Olivine, M.S. Thesis, Dep. of Geol.  
 396 Sci., Arizona State Univ., Tempe, Arizona.  
 397 Du Frane, W. L. (2010), Hydrogen in the Upper Mantle: Diffusion and Effects on Olivine  
 398 Transformation Kinetics, Ph.D. Diss., Sch. Earth Space Explor., Arizona State Univ., Tempe,  
 399 Arizona.  
 400 Du Frane, W. L., J. J. Roberts, D. A. Toffelmier, and J. A. Tyburczy (2005), Anisotropy of  
 401 electrical conductivity in dry olivine, *Geophys. Res. Lett.*, *32*, 24315, doi:  
 402 10.1029/2005GL023879.  
 403 Evans, R. L., G. Hirth, K. Baba, D. Forsyth, A. Chave, and R. Mackie (2005), Geophysical  
 404 evidence from the MELT area for compositional controls on oceanic plates, *Nature*,  
 405 *437*(7056), 249-252.  
 406 Filloux, J. H. (1980), Magnetotelluric Soundings over the Northeast Pacific May Reveal Spatial  
 407 Dependence of Depth and Conductance of the Asthenosphere, *Earth Planet. Sci. Lett.*, *46*(2),  
 408 244-252.

409 Hauri, E., J. H. Wang, J. E. Dixon, P. L. King, C. Mandeville, and S. Newman (2002), SIMS  
 410 analysis of volatiles in silicate glasses 1. Calibration, matrix effects and comparisons with  
 411 FTIR, *Chem. Geol.*, 183, 99-114.

412 Hirschmann, M. M., C. Aubaud, and A. C. Withers (2005), Storage capacity of H<sub>2</sub>O in  
 413 nominally anhydrous minerals in the upper mantle, *Earth Planet. Sci. Lett.*, 236(1-2), 167-181.

414 Huang, X. G., Y. S. Xu, and S. I. Karato (2005), Water content in the transition zone from  
 415 electrical conductivity of wadsleyite and ringwoodite, *Nature*, 434(7034), 746-749.

416 Ichiki, M., M. Uyeshima, H. Utada, G. Z. Zhao, J. Tang, and M. Z. Ma (2001), Upper mantle  
 417 conductivity structure of the back-arc region beneath northeastern China, *Geophys. Res. Lett.*,  
 418 28(19), 3773-3776.

419 Ingrin, J., and H. Skogby (2000), Hydrogen in nominally anhydrous upper-mantle minerals:  
 420 concentration levels and implications, *Eur. J. Mineral.*, 12(3), 543-570.

421 Inoue, T., H. Yurimoto, and Y. Kudoh (1995), Hydrous modified spinel, Mg<sub>1.75</sub>SiH<sub>0.5</sub>O<sub>4</sub> - a new  
 422 water reservoir in the mantle transition region, *Geophys. Res. Lett.*, 22(2), 117-120.

423 Jacobsen, S.D. and S. van der Lee, (2006), Eds., *Earth's Deep Water Cycle*, *Geophys. Monogr.*  
 424 *Ser.*, vol. 168, AGU, Washington, D.C.

425 Karato, S. (1990), The role of hydrogen in the electrical-conductivity of the upper mantle,  
 426 *Nature*, 347(6290), 272-273.

427 Karato, S. (2006), Influence of hydrogen-related defects on the electrical conductivity and plastic  
 428 deformation of mantle minerals: a critical review, in *Earth's Deep Water Cycle*, *Geophys.*

429 *Monogr. Ser.*, edited by S.D. Jacobsen and S. van der Lee, vol. 168, pp. 113-129, AGU,  
 430 Washington, D.C.

431 Keppler, H., and J. R. Smyth (2006), Water in Nominally Anhydrous Minerals, *Rev.Mineral.*  
 432 *Geochem.*, vol 62., Mineral. Soc. Amer., Washington, D.C.

433 Koga, K., E. Hauri, M. Hirschmann, and D. Bell (2003), Hydrogen concentration analyses using  
 434 SIMS and FTIR: Comparison and calibration for nominally anhydrous minerals, *Geochem.*,  
 435 *Geophys.*, *Geosys.*, 4, 1019, doi: 10.1029/2002GC000378.

436 Kohlstedt, D. L., H. Keppler, and D. C. Rubie (1996), Solubility of water in the alpha, beta and  
 437 gamma phases of (Mg,Fe)(2)SiO4, *Contrib. Mineral. Petrol.*, 123(4), 345-357.

438 Kohlstedt, D. L., and S. J. Mackwell (1998), Diffusion of hydrogen and intrinsic point defects in  
 439 olivine, *Z. Phys. Chem.*, 207, 147-162.

440 Kohlstedt, D.L. and S.J. Mackwell (1999), Solubility and diffusion of „water“ in silicate  
 441 minerals, in *Microscopic Properties and Processes in Minerals*, edited by K. Wright and R.  
 442 Catlow (Eds.), pp. 539-559, Kluwer Acad. Pub., London, UK.

443 Leibecker, J., A. Gatzemeier, M. Honig, O. Kuras, and W. Soyer (2002), Evidence of electrical  
 444 anisotropic structures in the lower crust and the upper mantle beneath the Rhenish Shield,  
 445 *Earth Planet. Sci. Lett.*, 202(2), 289-302.

446 Lizarralde, D., A. Chave, G. Hirth, and A. Schultz (1995), Northeastern Pacific Mantle  
 447 Conductivity Profile from Long-Period Magnetotelluric Sounding Using Hawaii-to-California  
 448 Submarine Cable Data, *J. Geophys. Res. [Solid Earth]*, 100(B9), 17837-17854.

449 Manthilake, M., T. Matsuzaki, T. Yoshino, S. Yamashita, E. Ito, and T. Katsura (2009),  
 450 Electrical conductivity of wadsleyite as a function of temperature and water content, *Phys.*  
 451 *Earth Planet. Inter.*, 174(1-4), 10-18.  
 452 Mosenfelder, J. L., N. I. Deligne, P. D. Asimow, and G. R. Rossman (2006), Hydrogen  
 453 incorporation in olivine from 2-12 GPa, *Am. Mineral.*, 91(2-3), 285-294.  
 454 Misener, D. J. (1973), Cationic diffusion in olivine to 1400°C and 35 kbar, in *Geochemical*  
 455 *Transport and Kinetics*, edited by A. W. Hofmann, B. J. Giletti, H. S. Yoder, Jr. and R. A.  
 456 Yund, *Carnegie Inst. Wash. Publ.*, 634, Washington, D. C.  
 457 Oldenburg, D. W. (1981), Conductivity Structure of Oceanic Upper Mantle beneath the Pacific  
 458 Plate, *Geophys. J. R. Astron. Soc.*, 65(2), 359-394.  
 459 Olsen, N. (1999), Long-period (30 days-1 year) electromagnetic sounding and the electrical  
 460 conductivity of the lower mantle beneath Europe, *Geophys. J. Int.*, 138(1), 179-187.  
 461 Paterson, M. S. (1982), The determination of hydroxyl by infrared-absorption in quartz, silicate-  
 462 glasses and similar materials, *Bull. Mineral.*, 105(1), 20-29.  
 463 Pitzer, K. S., and S. M. Sterner (1994), Equations of state valid continuously from zero to  
 464 extreme pressures for H<sub>2</sub>O and CO<sub>2</sub>, *J. Chem. Phys.*, 101(4), 3111-3116.  
 465 Poe, B. T., C. Romano, F. Nestola, and J. R. Smyth (2010), Electrical conductivity anisotropy of  
 466 dry and hydrous olivine at 8 GPa, *Phys. Earth Planet. Inter.*, 181(3-4), 103-111.  
 467 Roberts, J. J., and A. G. Duba (1995), Transient electrical response of San Quintin dunite as a  
 468 function of oxygen fugacity changes: information about charge-carriers, *Geophys. Res. Lett.*,  
 469 22(4), 453-456.

470 Romano, C., B. T. Poe, J. A. Tyburczy, and F. Nestola (2009), Electrical conductivity of hydrous  
 471 wadsleyite, *Eur. J. Mineral.*, *21*(3), 615-622.  
 472 Sato, H. (1986), High-temperature AC electrical-properties of olivine single-crystal with varying  
 473 oxygen partial-pressure - implications for the point-defect chemistry, *Phys. Earth Planet.*  
 474 *Inter.*, *41*(4), 269-282.  
 475 Schock, R. N., A. G. Duba, and T. J. Shankland (1989), Electrical-Conduction in Olivine, *J.*  
 476 *Geophys. Res. [Solid Earth Planets]*, *94*(B5), 5829-5839.  
 477 Shankland, T. J., and H. S. Waff (1977), Partial Melting and Electrical-Conductivity Anomalies  
 478 in Upper Mantle, *J. Geophys. Res.*, *82*(33), 5409-5417.  
 479 Shankland, T. J., R. J. Oconnell, and H. S. Waff (1981), Geophysical Constraints on Partial Melt  
 480 in the Upper Mantle, *Rev. Geophys.*, *19*(3), 394-406.  
 481 Simpson, F. (2002), A comparison of electromagnetic distortion and resolution of upper mantle  
 482 conductivities beneath continental Europe and the Mediterranean using islands as windows,  
 483 *Phys. Earth Planet. Inter.*, *129*(1-2), 117-130.  
 484 Simpson, F., and A. Tommasi (2005), Hydrogen diffusivity and electrical anisotropy of a  
 485 peridotite mantle, *Geophys. J. Int.*, *160*(3), 1092-1102.  
 486 Stalder, R., and H. Behrens (2006), D/H exchange in pure and Cr-doped enstatite: implications  
 487 for hydrogen diffusivity, *Phys. Chem. Miner.*, *33*(8-9), 601-611.  
 488 Tarits, P., S. Hautot, and F. Perrier (2004), Water in the mantle: Results from electrical  
 489 conductivity beneath the French Alps, *Geophys. Res. Lett.*, *31*, L06612, doi:  
 490 10.1029/2003GL019277.

491 Tenner, T. J., M. M. Hirschmann, A. C. Withers, and R. L. Hervig (2009), Hydrogen partitioning  
 492 between nominally anhydrous upper mantle minerals and melt between 3 and 5 GPa and  
 493 applications to hydrous peridotite partial melting, *Chem. Geol.*, 262(1-2), 42-56.  
 494 Wang, D. J., M. Mookherjee, Y. S. Xu, and S. Karato (2006), The effect of water on the  
 495 electrical conductivity of olivine, *Nature*, 443(7114), 977-980.  
 496 Xu, Y. S., B. T. Poe, T. J. Shankland, and D. C. Rubie (1998), Electrical conductivity of olivine,  
 497 wadsleyite, and ringwoodite under upper-mantle conditions, *Science*, 280(5368), 1415-1418.  
 498 Yoshino, T., T. Matsuzaki, S. Yamashita, and T. Katsura (2006), Hydrous olivine unable to  
 499 account for conductivity anomaly at the top of the asthenosphere, *Nature*, 443(7114), 973-976.  
 500 Yoshino, T., T. Matsuzaki, A. Shatskiy, and T. Katsura (2009), The effect of water on the  
 501 electrical conductivity of olivine aggregates and its implications for the electrical structure of  
 502 the upper mantle, *Earth Planet. Sci. Lett.*, 288(1-2), 291-300.  
 503 Yoshino, T., M. Laumonier, E. McIsaac, and T. Katsura (2010), Electrical conductivity of  
 504 basaltic and carbonatite melt-bearing peridotites at high pressures: Implications for melt  
 505 distribution and melt fraction in the upper mantle, *Earth Planet. Sci. Lett.*, 295(3-4), 593-602.  
 506 Zhang, S. Q., and S. Karato (1995), Lattice preferred orientation of olivine aggregates deformed  
 507 in simple shear, *Nature*, 375(6534), 774-777.  
 508 Zhao, Y. H., S. B. Ginsberg, and D. L. Kohstedt (2004), Solubility of hydrogen in olivine:  
 509 dependence on temperature and iron content, *Contrib. Mineral. Petrol.*, 147(2), 155-161.

510 **Table 1.** Olivine and enstatite diffusion coefficient results at 2 Gpa.

Sample	Run	Duration (hrs) <sup>†</sup>	T (°C) <sup>‡</sup>	Orientation	Experiment	LogD
ol	PC25	17/48/1	750	[100]	<sup>2</sup> H- <sup>1</sup> H	-12.3 (0.3)
ol	PC25	17/48/1	750	[010]	<sup>2</sup> H- <sup>1</sup> H	< -15 (1*)
ol	PC25	17/48/1	750	[001]	<sup>2</sup> H- <sup>1</sup> H	< -13 (1*)
ol	PC28	16.5/26/0.25	800	[100]	<sup>2</sup> H- <sup>1</sup> H	-11.7 (0.1)
ol	PC28	16.5/26/0.25	800	[010]	<sup>2</sup> H- <sup>1</sup> H	< -14 (1*)
ol	PC28	16.5/26/0.25	800	[001]	<sup>2</sup> H- <sup>1</sup> H	< -14 (1*)
ol	PC30	16.5/16/.17	850	non-oriented	<sup>2</sup> H- <sup>1</sup> H	-12.5 (1*)
ol	PC30	16.5/16/.17	850	non-oriented	<sup>2</sup> H- <sup>1</sup> H	-12.9 (1*)
ol	PC30	16.5/16/.17	850	non-oriented	<sup>2</sup> H- <sup>1</sup> H	-13.0 (1*)
ol	PC33	17/18/0.17	900	[100]	<sup>2</sup> H- <sup>1</sup> H	-11.2 (0.1)
ol	PC33	17/18/0.17	900	[010]	<sup>2</sup> H- <sup>1</sup> H	< -13 (1*)
ol	PC33	17/18/0.17	900	[001]	<sup>2</sup> H- <sup>1</sup> H	-12.0 (0.2)
en	PC25	17/48/1	750	non-oriented	<sup>2</sup> H- <sup>1</sup> H	-13.0 (0.2)
en	PC25	17/48/1	750	non-oriented	<sup>2</sup> H- <sup>1</sup> H	-12.8 (0.5)
en	PC28	16.5/26/0.25	800	non-oriented	<sup>2</sup> H- <sup>1</sup> H	-13.2 (0.1)
en	PC33	17/18/0.17	900	orthogonal 1	<sup>2</sup> H- <sup>1</sup> H	-11.7 (0.3)
en	PC33	17/18/0.17	900	orthogonal 2	<sup>2</sup> H- <sup>1</sup> H	-11.7 (0.3)
en	PC33	17/18/0.17	900	orthogonal 3	<sup>2</sup> H- <sup>1</sup> H	-12.0 (0.3)

511 <sup>†</sup> Durations are presented for dry/wet/exchange anneals.

512 <sup>‡</sup> T given is same for both wet and exchange anneals. T = 1300 °C for all dry anneals.

513 \* Error estimated because of limited data, all other errors are one standard deviation from least  
514 squares fitting solutions to equation 5.



515

516 **Figure 1.** Reflected light micrograph of sample PC33 showing array of craters from SIMS spot  
517 analyses from the (100) edge of the crystal.

518

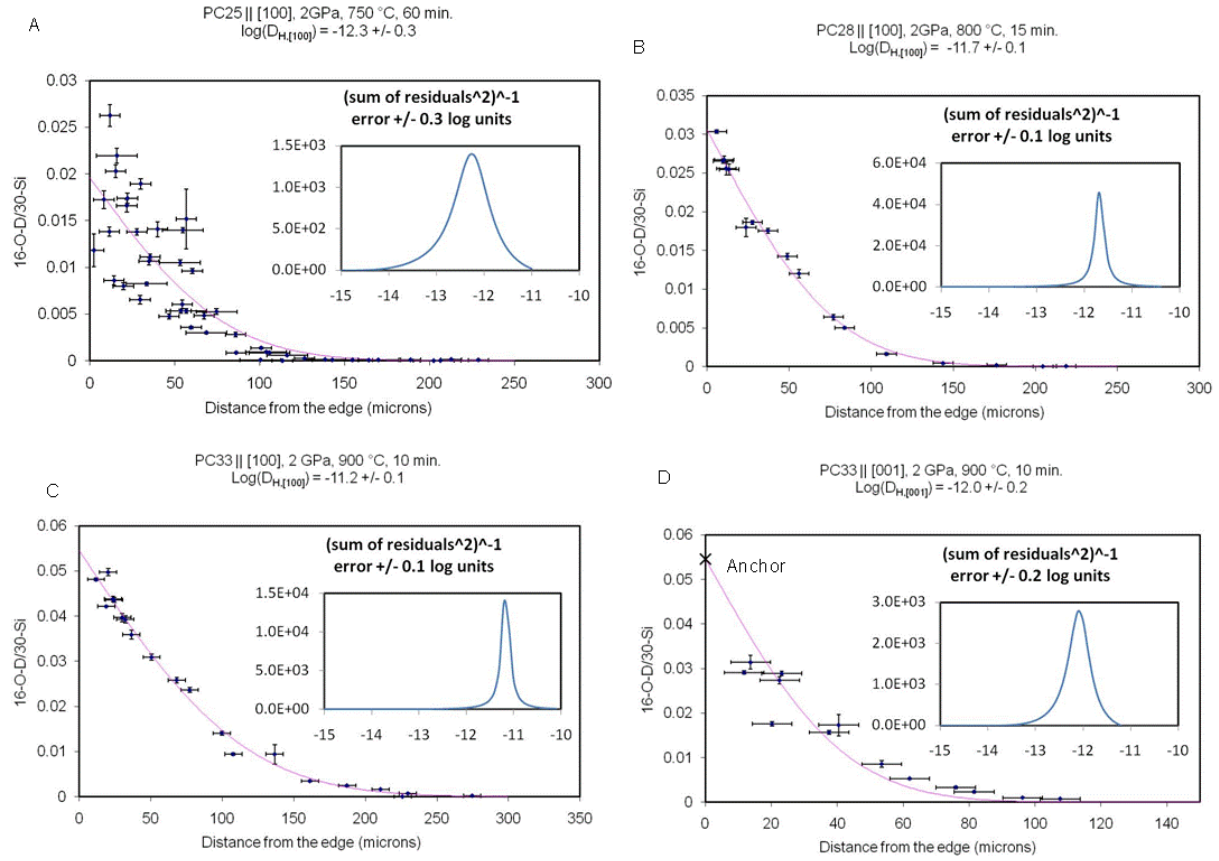


**Figure 2.** Diffusion profiles for  $^2\text{H}$ - $^1\text{H}$  exchange at 2 GPa in olivine pre-saturated with  $^1\text{H}$ . a) 750, [100]; b) 800, [100]; c) 900 °C, [100]; d) 900 °C, [001]. Insets show the sum of fitting residuals squared, with fitting errors calculated as one standard deviation from each solution.

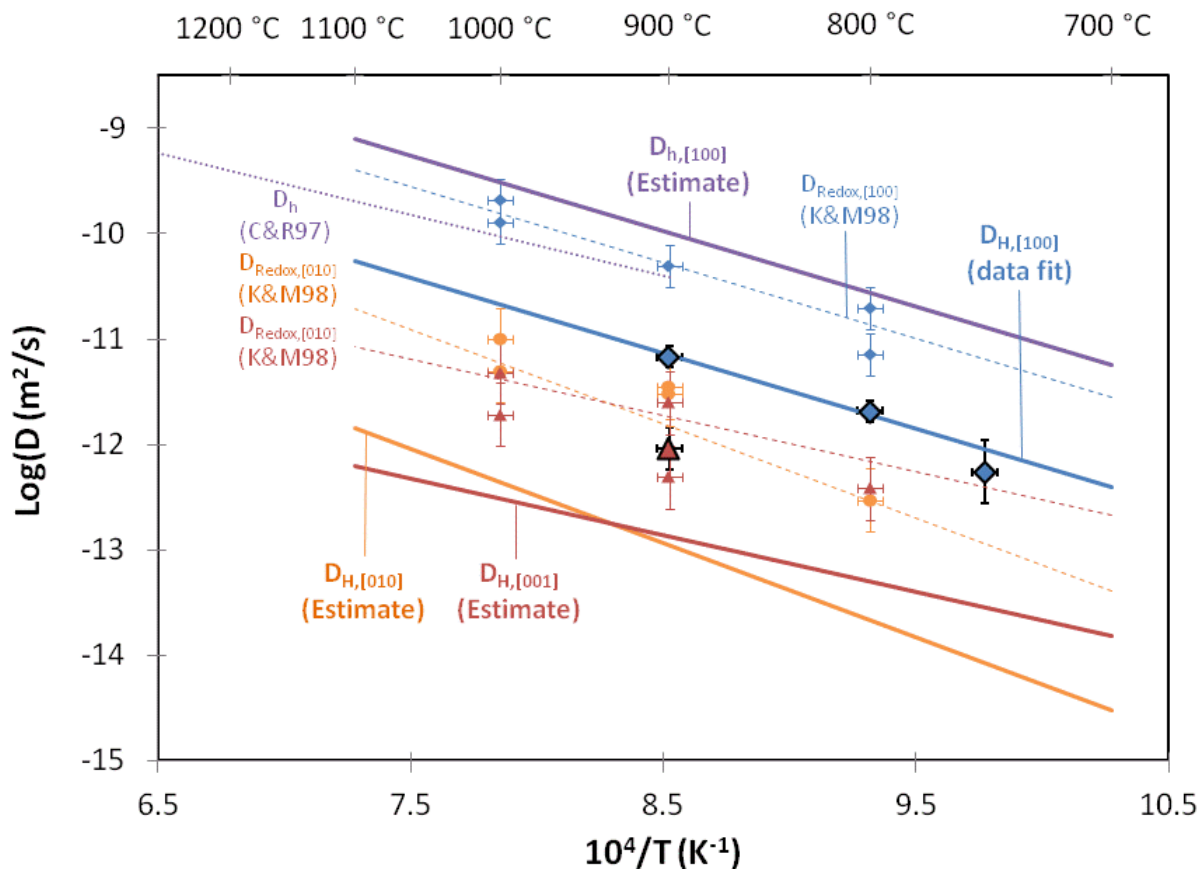


**Figure 3.** Arrhenius plot of diffusion coefficients versus reciprocal temperature:  $D_{H,[100]}$  – outlined blue diamonds.  $D_{H,[001]}$  – outlined red triangle. Data fit of  $D_{H,[100]}$  - solid blue line. Calculations of  $D_{h,[100]}$  - solid purple line,  $D_{h,[010]}$  - solid orange line, and  $D_{h,[001]}$  - solid red line. Also shown are chemical diffusion coefficients based on redox exchange experiments -  $D_{\text{Redox}}$  (K&M98); *Kohlstedt and Mackwell* [1998] ([100] – blue diamonds, [010] – orange circles, [001] – red triangles; with data fits in corresponding colors), and small polaron diffusion coefficient calculated from electrical properties of dry, polycrystalline San Quintin dunite -  $D_h$  (C&R97); *Constable and Roberts* [1997] (dashed purple line).

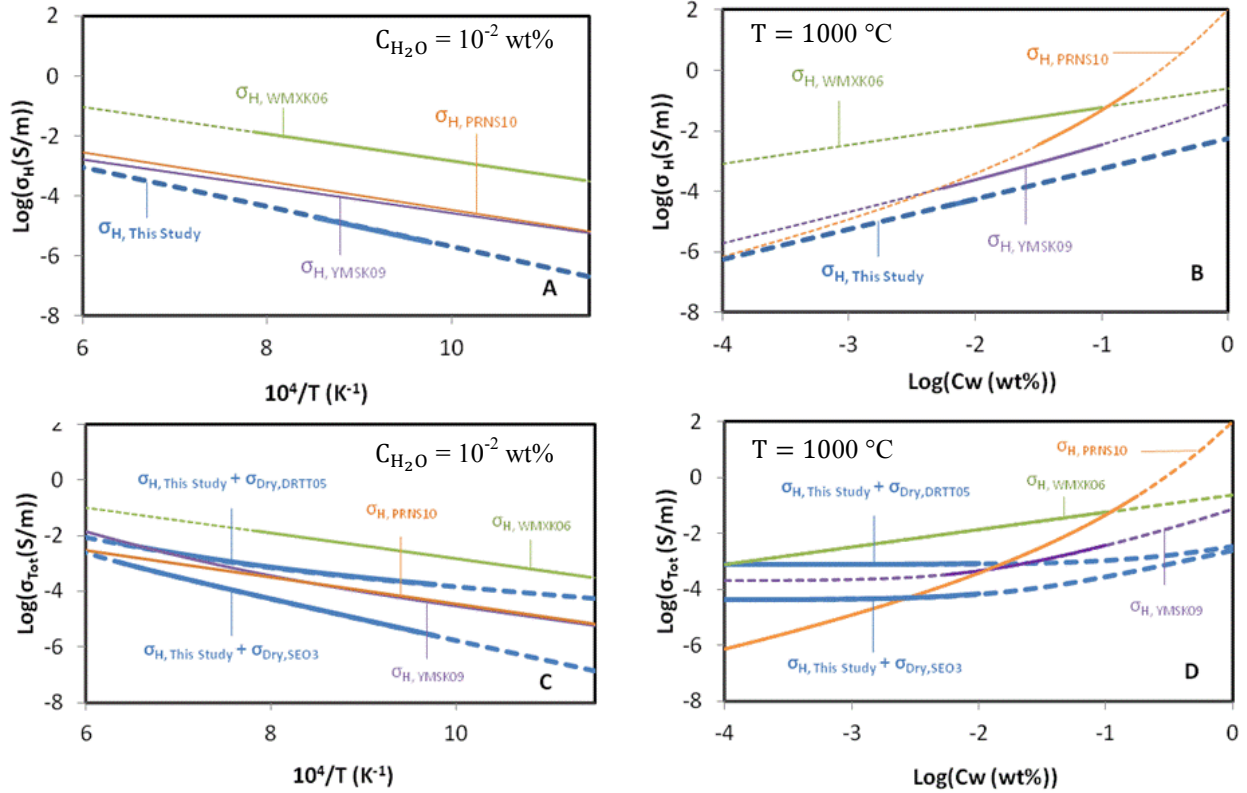


**Figure 4.**  $\sigma_H$  (A, B),  $\sigma_{Tot}$  (C, D) using  $\sigma_{Dry}$  data from *Du Frane et al.* [2005] or SEO3 model from *Constable* [2006] as a function of  $1/T$  and  $C_{H_2O}$  of hydrous olivine from this study (blue lines), *Wang et al.* [2006] (WMXK06 - green line), *Yoshino et al.* [2009] (YMSK09 - purple line), and *Poe et al.* [2010] (PRNS10 - orange line). Dashed lines indicate extrapolation beyond experimental ranges of  $T$  and  $C_{H_2O}$  for each study.

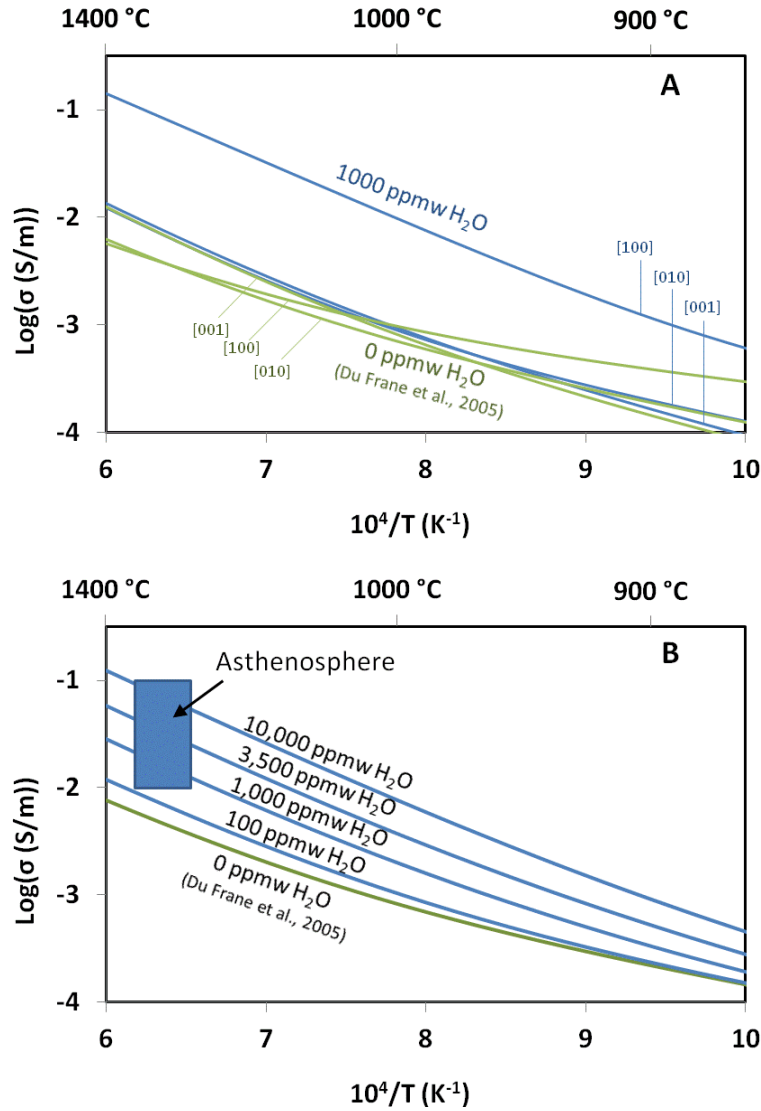


**Figure 5.** Model of  $\sigma_{Tot}$  of hydrous olivine aggregate (this study) for various  $C_{H_2O}$ , versus reciprocal temperature. A)  $\sigma_{Tot,[100]}$ ,  $\sigma_{Tot,[010]}$ , and  $\sigma_{Tot,[001]}$ . B) Geometric means of  $\sigma_{Tot,[100]}$ ,  $\sigma_{Tot,[010]}$ , and  $\sigma_{Tot,[001]}$ . The blue, shaded region shows  $\sigma$  values observed at asthenospheric depths, with the high end of the range observed beneath the Eastern Pacific rise and the low end observed beneath continental lithosphere [Lizarralde *et al.*, 1995; Olsen, 1999; Ichiki *et al.*, 2001; Tarits *et al.*, 2004; Baba *et al.*, 2006].